VTT Technical Research Centre of Finland

Wheel load reconstruction using strain gauge measurements on the bogie frame for strain prediction and fatigue assessment

Nieminen, Vesa; Tuohineva, Antero; Autio, Maija

Published in:
International Journal of Fatigue

DOI:
10.1016/j.ijfatigue.2023.107533

Published: 01/05/2023

Document Version
Publisher's final version

International Journal of Fatigue 170 (2023) 107533

Contents lists available at ScienceDirect

International Journal of Fatigue

journal homepage: www.elsevier.com/locate/ijfatigue

Wheel load reconstruction using strain gauge measurements on the bogie frame for strain prediction and fatigue assessment

Vesa Nieminen [a,*], Antero Tuohineva [b], Maija Autio [b]

[a] VTT Technical Research Centre of Finland Ltd, Tietotie 4C, FI-02150 Espoo, Finland
[b] Skoda Transtech Oy, Elektroniikkatie 2, FI-90590 Oulu, Finland

ARTICLE INFO

Keywords:
Load reconstruction
Bogie frame
Virtual sensing
Optimal sensor placement
Fatigue damage

ABSTRACT

Knowledge of actual wheel-rail contact forces under a service environment is critical for fatigue damage prediction of rail vehicle bogies. This paper presents a method for reconstructing operational wheel loads based on the strain gauge measurements on the bogie of a tram. The strain gauge placement is solved as an optimisation problem, and the actual load–strain relationship is verified by physical calibrations. A novel calibration arrangement is presented to produce linearly independent load cases for a fully equipped bogie. A good correlation of the reconstructed operational stresses with the measured stresses indicated that the identified loads are valid for fatigue assessment.

1. Introduction

Virtual sensing and real-time information on the structural behaviour of vehicles during operation provides essential information of structural integrity and is an important part of the intelligence of vehicles. For railway vehicles, measuring wheel loads while running provides valuable information about loads to the bogie structure and also the quality of the track. In addition, knowledge of wheel-rail contact forces during operation is essential from a running safety point of view. However, the direct measurement of wheel loads is difficult in practice. It has been recognised that, in general, the standardised determination of the service spectrum and the derivation of the real load spectrum for rolling stock applications is not sufficiently well developed [1,2]. The assessment of fatigue strength of a bogie frame is traditionally based on the endurance strength approach in terms of constant amplitude loads and a defined number of cycles. Another approach is to define the stress-time history based on variable amplitude load cases and use the cumulative damage approach. In that case, the load history can be generated, for example, by using multi-body simulation (MBS) [3]. In this approach, actual operational loads are considered, and the fatigue assessment can be performed for a specific rail network. However, it is challenging to create a stress-time history that corresponds sufficiently to reality, including, e.g., a wide variety of track geometry details and a huge number of unknown track irregularities.

Prediction of operational stresses and fatigue damage based on measured service loads provides actual service loads and their characteristics for specific railway network. This approach allows prediction of the fatigue damage of bogies under similar application conditions. Different methods have recently been developed and applied to predict the operational load and fatigue damage of a bogie of the railway vehicles. Wu et al. have applied a frequency domain transfer function method based on axle box acceleration measurements to estimate fatigue damage of the bogie frame of a rail vehicle [4]. Wang et al. [5] and Ji et al. [6] measured the service loads and dynamic stresses of a high-speed train bogie under operational conditions with strain gauges installed in high stress response regions in order to measure bending or tension loads on specific locations of the structure. Static load–strain transfer coefficients were estimated by calibration measurements in a test rig. However, strain gauge placement optimisation was not applied in this study, which may be needed to minimise, e.g., cross-coupling effects in the case of complex structural geometries.

Wheel-rail interaction and measurement methods for wheel-rail contact forces during vehicle operation have been investigated in several studies. Matsumoto et al. applied non-contact displacement sensors installed on the non-rotating parts of a bogie to measure lateral and vertical wheel forces [7]. In this study, the bending deflection of a wheel was measured by a gap sensor mounted on the axle bearing box, and vertical force was measured from the displacement of a primary suspension spring by an LVDT displacement sensor. However, lateral movement of the wheelset relative to the axle box and possible

* Corresponding author at: VTT Technical Research Centre of Finland, Tietotie 4C, FI-02150 Espoo, Finland.
E-mail address: vesa.nieminen@vtt.fi (V. Nieminen).

https://doi.org/10.1016/j.ijfatigue.2023.107533
Received 16 November 2022; Received in revised form 12 January 2023; Accepted 17 January 2023
Available online 20 January 2023

misalignment between the wheel and the axle introduces measurement error in this approach and must be compensated. Urda et al. [8] presented a scaled dynamometric wheelset, where vertical forces were also calculated from deflections experienced by the primary suspension elements, measured by two displacement laser sensors. Lateral forces were measured by strain gauges installed on the wheel web and also by displacement lasers installed on the bearing box.

Indirect methods to predict wheel forces have also been studied recently. Xia et al. [9] developed an inverse wagon model to predict wheel-rail contact forces from measured wagon body responses only. Sun et al. [10] introduced a two-dimensional inverse wagon model that was used to predict wheel-rail dynamic forces based on acceleration measurements from a car body and bogie frame. Weia et al. [11] presented an inverse model-based method for the wheel-rail force measurement based on acceleration measurements on the bearing box and the relative displacements of the primary suspension. However, the main focus of these studies has not been on the fatigue assessment of a bogie, and these methods have not been validated by operational strain measurements on the bogie frame, for example. It is evident that model uncertainties have an impact on the accuracy of these type of model-based methods.

In this study, a method for reconstructing wheel loads by using strain gauge measurements from optimised locations of the bogie frame structure is developed. The methodology was applied to the bogie of a tram. Just by measuring stresses in some optimally selected locations of a bogie frame, the wheel loads of a vehicle can be identified and stresses at any point of the whole bogie structure can be recovered. Online measurements of these few stress measuring locations can be easily performed, and thus real-time information on operational loads of bogie structure and track condition can be obtained. A novel calibration arrangement is presented to produce linearly independent load cases for the fully equipped bogie, which is essential for experimental determination of influence coefficients between the strain responses and the external loads.

The method includes the following steps: First, optimal strain gauge locations and angular orientations are chosen by using an optimisation procedure based on FEM simulations. Then, by calibration measurements with linearly independent load cases, the load-stress relationship of chosen measuring locations is measured, and an influence coefficient matrix is determined. Finally, in track tests, the quality of the developed model is verified by comparing the reconstructed stress with a reference stress signal measured directly on the structure.

2. Methodology

In the case of complex structural geometries, it is very challenging or almost impossible to determine optimal strain gauge locations and the minimum number of gauges needed for load identification based on engineering judgement only. In the case of simple structures resembling a cantilevered beam, for example, the gauge location may be intuitive under certain loading conditions, but for complex structures the optimal gauge placement is no longer evident. Therefore, the strain gauge placement must be solved as an optimisation problem to eliminate errors due to cross-coupling effects, for example. The applied methodology is briefly presented in this chapter. An overview of the whole operational stress recovery process is shown in Fig. 1.

In a quasi-static linear elastic problem, the relationship between strains ε of the structure caused by external loads F can be expressed by:

$$\{F\} = \{\varepsilon\}[\mathbf{C}] \tag{1}$$

where F is $1 \times k$ row vector of external loads, ε is $1 \times m$ row vector of strains, and $\mathbf{C}$ is $m \times k$ matrix of influence coefficients. In this case, k represents the number of load components to be identified, and m represents the number of strain gauges ($m > k$). To identify elements of $\mathbf{C}$, n linearly independent load cases should be performed ($n \geq k$), either from a numerical model (e.g. the FE-model) or physical calibration measurements. The Eq. (1) becomes:

$$\mathbf{F} = \varepsilon\mathbf{C} \tag{2}$$

where $\mathbf{F}$ is the $n \times k$ matrix of loads of n calibration cases and $\boldsymbol{\varepsilon}$ is the $n \times m$ matrix of corresponding strains. The influence coefficients can now be estimated as:

$$\widehat{\boldsymbol{C}} = \left(\varepsilon^T\varepsilon\right)^{-1}\varepsilon^T\boldsymbol{F} = \varepsilon^{\dagger}\boldsymbol{F} \tag{3}$$

where $\widehat{\mathbf{C}}$ denotes the least squares estimate of the unknown influence coefficient matrix and $(.)^{\dagger}$ represents the Moore-Penrose pseudoinverse. It is assumed here that the confidence of strains at all locations are equal, and variances of the strain noise are also equal. The error covariance matrix of the weighted least squares estimate of $\widehat{\mathbf{C}}$ is:

$$\sum_{\widehat{C}} = \left(\varepsilon^T\varepsilon\right)^{-1} \tag{4}$$

Because $\mathbf{F}$ is a linear combination of $\mathbf{C}$ and measured strains $\boldsymbol{\varepsilon}$ according to Eq. (2), minimising variance of $\widehat{\mathbf{C}}$ also results in the minimisation of variance of the load estimates $\widehat{\mathbf{F}}$. The inverse of a matrix can be calculated by dividing the adjoint of the matrix by the determinant of the matrix; therefore, the objective function in strain gauge placement optimisation was defined as maximisation of the determinant $|\varepsilon^T\varepsilon|$ (the so-called D-optimal design technique). In addition, the condition number of matrix $\boldsymbol{\varepsilon}$ is a good evaluation criterion for the quality of the gauge placement result. The condition number can be considered as a measure of stability of $\widehat{\mathbf{C}}$; the lower value indicates insensitivity to measurement noise and gauge placement accuracy, and vice versa.

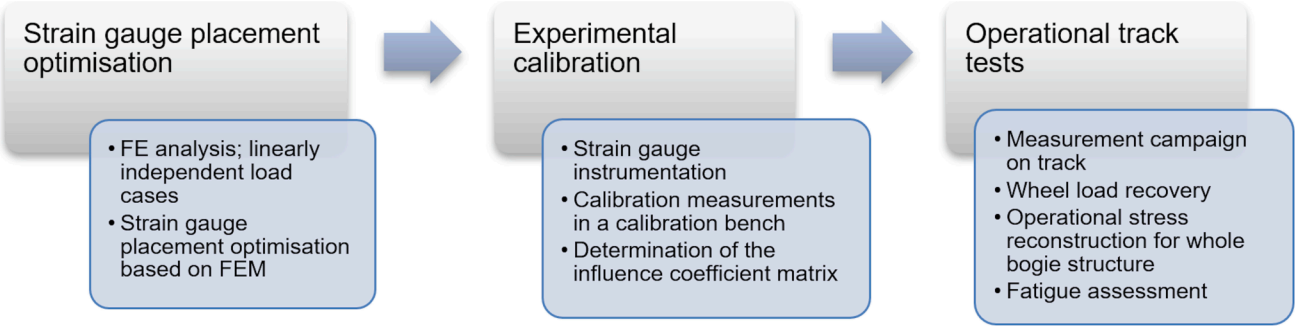

Fig. 1. Overview of the operational stress recovery process.

2.1. Gauge placement optimisation procedure

Optimal strain gauge locations and angular orientations were optimised based on the FEM simulations. Loads were applied separately to the structure corresponding the loads to be estimated, and the resulting strain fields from each of the load cases were calculated. The elements on the surface of the structure were defined as the candidate strain gauge locations for the optimisation. Because strain gauge sensitivity also depends on the gauge angular orientation, the strain tensors for each candidate strain gauge locations must be transformed to determine strain values for different gauge orientations. Orientations of all the candidate strain gauges were varied during optimisation in order to discover optimal locations as well as optimal orientations of the strain gauges. Each combination of location and angular orientation of m strain gauges formed a subset of all possible combinations and represented a candidate set for inclusion in the matrix $\boldsymbol{\varepsilon}$. An iterative sequential-exchange algorithm was utilised to select optimum sensor locations and orientations as follows [12,13]:

i. An initial subset of m gauge locations and orientations was selected randomly from the surface element set and an initial value for $|\varepsilon^T\varepsilon|$ was evaluated.
ii. Utilising a forward sequential sensor placement scheme, one additional gauge location/orientation was added in turn to the selected gauge set, and the optimisation target function $|\varepsilon^T\varepsilon|$ was evaluated. The location/orientation leading to the largest increase in the target function was selected as an additional gauge.
iii. Utilising a backward sequential sensor placement scheme, one gauge location/orientation was removed in turn from the selected gauge set, and the location/orientation resulting design with the minimum possible degrease of $|\varepsilon^T\varepsilon|$ was removed from the optimum gauge set.
iv. Steps ii) and iii) were repeated until the target function $|\varepsilon^T\varepsilon|$ was not able to be further improved.

It should be noted that the chosen optimal strain gauge locations/orientations are not necessarily the same as most loaded locations in the structure, which are typically monitored in type tests.

Number of strain gauges should be greater than number of load components to be identified because equation (3) must be over-determined. However, in practice, due to measurement noise and inverse problem nature of equation (3), the number of strain gauges should clearly exceed the number of load components to avoid adverse errors in load estimates.

2.2. Utilisation of physical calibrations

The numerical model always includes uncertainties and idealisations, such as, in this case, an assumption of linear behaviour. In addition, strain gauge measurements include uncertainties related to gauge placement and orientation accuracy, for example. Therefore, it is important to determine the actual relationship between the strains and the external loads, i.e., $\widehat{\mathbf{C}}$, by physical calibrations. Calibration load cases should be linearly independent, which means that the matrix $\mathbf{F}$ in Eq. (3) should be a diagonal matrix in an ideal case, where elements of the main diagonal are applied calibration loads.

Identified operational loads can be validated by installing additional independent reference strain gauges, which will not be used for the identification of the matrix $\widehat{\mathbf{C}}$. The strains for single reference strain gauge during the physical calibrations can be expressed by:

$$\{\varepsilon_{ref}\} = [\mathbf{F}]\{A\} \tag{5}$$

where ε_{ref} is $n \times 1$ column vector of reference strains at calibration cases and A is $n \times 1$ column vector of sensitivity coefficients. The sensitivity coefficients for each reference strain gauge can be estimated by:

$$\{\widehat{A}\} = \boldsymbol{F}^{\dagger}\{\varepsilon_{ref}\} \tag{6}$$

Reference strains during driving can now be reconstructed by substituting the estimated sensitivity coefficients (6) into Eq. (5). In this strain reconstruction phase, matrix $\mathbf{F}$ contains the identified wheel load component time histories, where each row contains identified load components at a single time step. Because the sensitivity coefficients for each reference strain gauge are identified from physical calibrations, the reconstructed reference strains can now be compared with the measured reference strains for validation of the identified loads. This comparison also gives information on contributions of each load component for the total reference strains. After validation of the identified operational loads, strains of the whole structure can now be recovered from Eq. (5) by applying sensitivity coefficients calculated by the FE-model for the unmeasured locations.

It should be noted that identified load estimates are based on linear static elastic equations, so they are valid only for static and quasi-static loading cases. In dynamic cases, the equation of motion can be expressed as:

$$\boldsymbol{M}\ddot{x} + \boldsymbol{D}\dot{x} + \boldsymbol{K}x = \boldsymbol{F}_{dyn} \tag{7}$$

where $\boldsymbol{M}$ is mass matrix, $\boldsymbol{D}$ is viscous damping matrix, $\boldsymbol{K}$ is stiffness matrix and $\boldsymbol{F}_{dyn}$ is external dynamic force. However, at a low frequency range, where elastic modes of the bogie frame can be ignored, the strain-based identified loads are related to the potential energy stored in the bogie frame, and they are the sum of external forces, inertia forces and damping forces according to the equation of the motion:

$$\boldsymbol{F}_{identified} = \boldsymbol{K}x = \boldsymbol{F}_{dyn} - \boldsymbol{M}\ddot{x} - \boldsymbol{D}\dot{x} \tag{8}$$

Therefore, the reconstructed strains calculated according to equation (5) are still valid at a low frequency range, where the elastic modes of the bogie frame can be ignored, as can be seen in the reconstructed reference stress histories presented in Section 3.2. The lower the frequency, the smaller the contribution of the inertia and damping forces for the total force balance of the system. Consequently, at frequencies near zero, the difference between the external dynamic force and the total identified force becomes small.

In cases where the elastic modes will be significantly excited during operation, the strain reconstruction in a dynamic frequency range can be carried out based on the modal superposition principle, i.e., mode shapes and modal coordinates. This approach can be applied based on the strain gauge measurements [12] or vibration measurements, such as acceleration measurements [14,15]. However, the sensor placement optimisation algorithm used must be adapted for the applied strain reconstruction method.

3. Experimental validation

The methodology was applied to the bogie of an MLRV03 Smart Artic X54 tram, see Fig. 2 and Fig. 3. The tram is manufactured by Skoda Transtech and it is used in the Helsinki railway network. It is a bi-directional low-floor tram, consisting of five modules, and there are four pivoting traction bogies. The test route in the validation track tests was fairly long (the duration was about one hour) and included different types of routes around the Helsinki railway network.

Fig. 2. MLRV03 Smart Artic X54 tram.

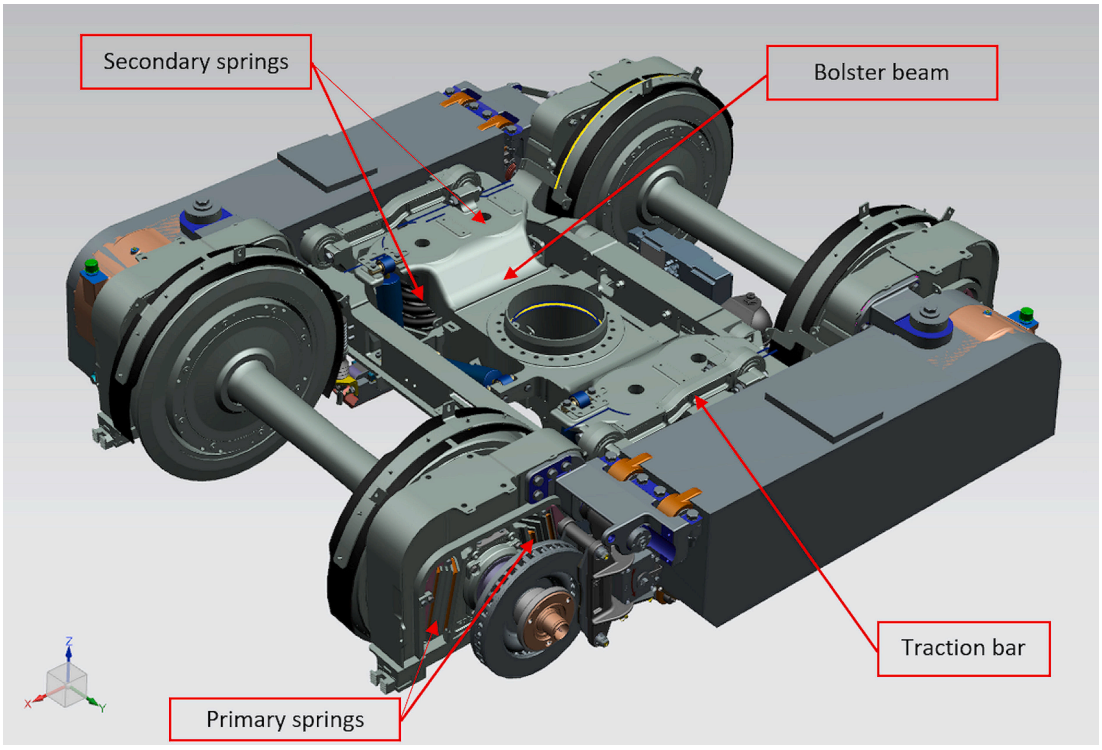

Fig. 3. Bogie of MLRV03 Smart Artic X54 tram and coordinate system used.

Before instrumentation, the strain gauge locations were optimised utilising the FE-model of the bogie frame, see Fig. 3 and Fig. 4. The elements on the surface of the bogie frame were defined as the candidate strain gauge locations for the optimisation. A total of ten independent loading cases were simulated: vertical (Z) as well longitudinal (X) loadings for all four wheels separately and transversal (Y) loadings for the right wheel of the front axle and the left wheel of the rear axle. The bogie frame was instrumented by 21 strain gauges in total at optimised locations, see Fig. 4. In addition, several additional reference strain gauges were installed.

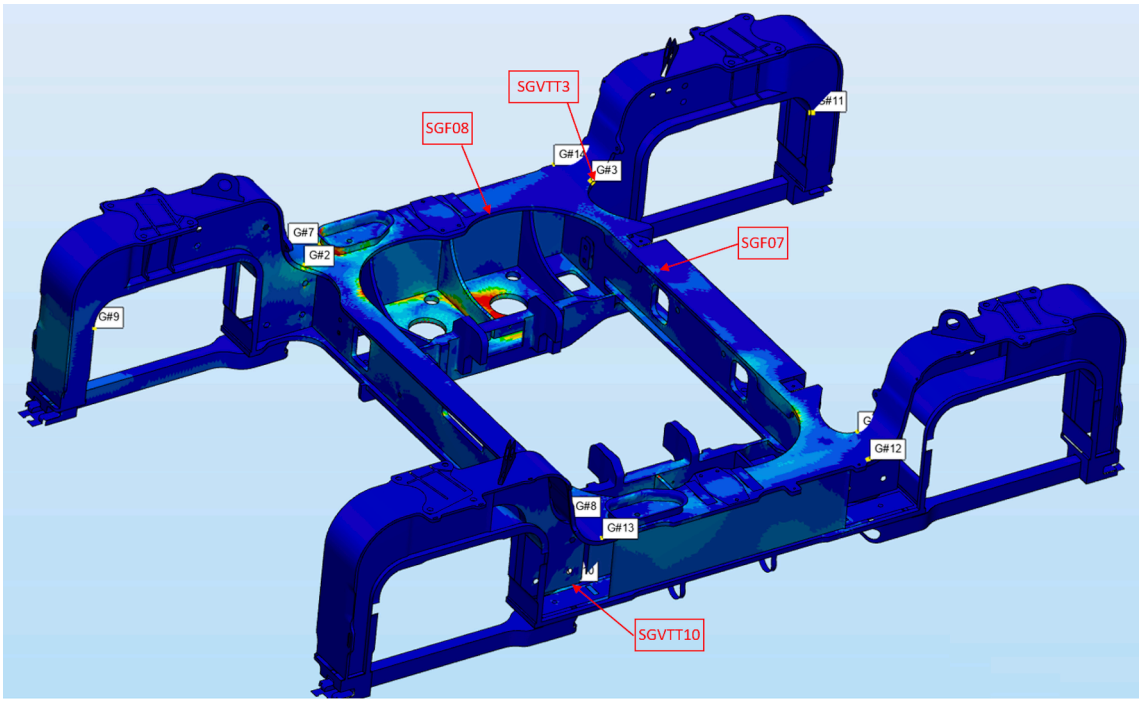

Fig. 4. FE-model of the bogie frame and part of the optimised strain gauge locations. The reference strain gauges used are shown in red.

3.1. Calibration measurements

Calibration measurements were conducted for a fully equipped bogie, see Fig. 3. Physical calibrations using external loads were carried out in the workshop, where the bogie was installed on the test rig. The bolster beam of the bogie was fixed to the test rig by a bolt joint. The calibration loads were measured by force transducers and strains were measured by strain gauges. A total of ten calibration cases were measured: vertical (Z) as well as longitudinal (X) loadings for all four wheels separately, and transversal (Y) loadings for the right wheel of the front axle and the left wheel of the rear axle. Thus, each calibration case corresponds to an individual external load component to be identified.

Calibration arrangements are presented in Fig. 5. A fully equipped bogie was fixed to the test rig from the bolster beam. The calibration force was produced by a hydraulic jacket. During calibrations, it is essential that the boundary conditions of the bogie frame correspond as closely as possible to normal operational conditions during driving. When the bogie was fixed to the test rig without external loading, the gravitational force of the tram modules was not present; therefore, primary and secondary springs were at the limits of their travel, due to preloading of the springs. In addition, the primary springs of the wheels have non-linear elastic behaviour. Consequently, this situation does not correspond to operational conditions and, therefore, the test arrangements were modified as follows.

All wheels were loaded by crane in a vertical direction via slings with a nominal operational load to reach nominal displacement for all primary (and secondary) spring elements. It is important that the load cases are linearly independent, which means that all load components, except the load under calibration, should remain as constant as possible during the calibrations. To produce linearly independent load cases, a specially designed lifting frame was applied between the slings and the crane. Support points of the lifting frame were designed so that in the vertical calibration case, vertical loads for all other wheels, except the wheel under calibration, remained equal during calibration, even though the bogie was tilted due to secondary spring deformations, see Fig. 5. Tilting moments of the lifting frame were balanced around the lifting point so that the tilting angle of the lifting frame and the bogie was approximately equal during calibration and consequently the vertical forces of the slings were also approximately equal. This was also verified by installing force transducers between the slings and the lifting frame. In addition, to reduce changes in the sling forces during calibrations, spring elements were installed between the slings and the lifting frame. The stiffness of these spring elements was approximately 25 times lower than the stiffness of the primary springs. In lateral and longitudinal calibration cases, all wheels were loaded in a vertical direction by slings with a nominal operational load. In these cases, the lifting point was in the middle of the lifting frame.

3.2. Results

Before estimating the influence coefficients from the calibration measurements, the linearity of the structure was checked. Fig. 6 shows samples of measured stresses as a function of the external calibration force. Moderate non-linear behaviour can be seen in the stress plots. The relationship between stress and calibration force was linearised for all strain gauges by least squares fit, and these linearised coefficients were used in the estimation of the influence coefficient matrix. The condition number of the experimental strain matrix ε was in this case 27, which can be considered acceptable. Heuristic evidence has been indicated that acceptable strain matrices have condition numbers of 50 or less [16].

Identified wheel loads during normal driving conditions and a comparison of reconstructed stresses with reference strain gauge measurements are presented in Fig. 7. The highest stress levels during validation track tests occurred on the bogie frame during this presented driving condition. Two different reconstructed stresses are presented in the figure: the reconstruction including vertical and lateral wheel loads for the reconstruction, and including vertical loads only. The presented signals are scaled with reference values due to confidentiality reasons:

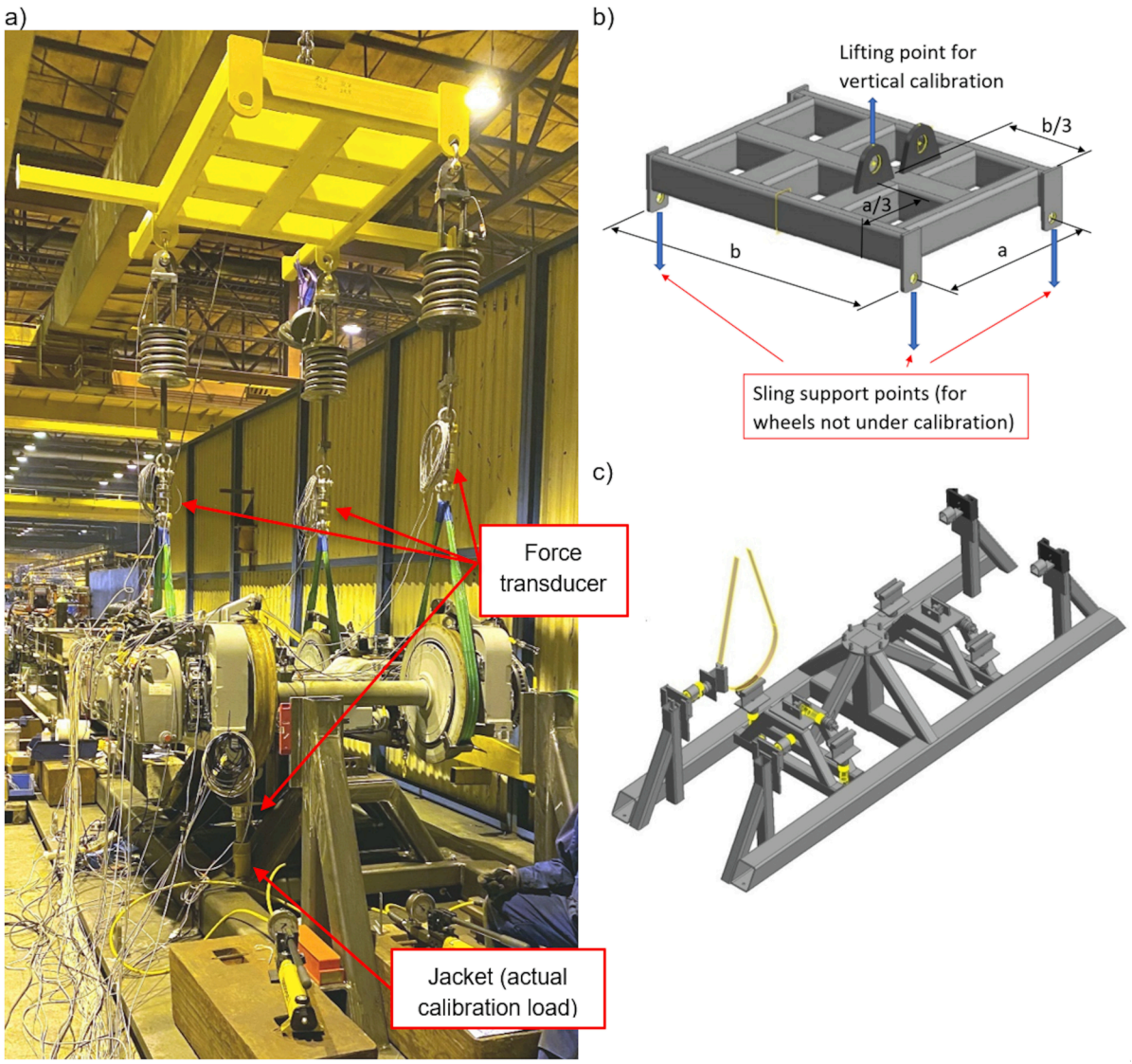

Fig. 5. Calibration arrangements for the vertical wheel load calibration case (a), lifting frame (b) and calibration test rig used (c). The test rig also includes supporting brackets for the lateral and longitudinal calibration loads.

F_{ref} is the average dynamic amplitude of the vertical load of the front left wheel (W1Z), and σ_{ref} is the measured average stress amplitude of strain gauge SGF07. The reference values are calculated from measurements of about one hour in length during normal driving. The comparison reveals that there are relatively small differences between these two reconstructed stresses except SGVTT10, which implies that the lateral forces have a limited impact on the bogie stresses. Naturally, the actual impact depends on the location on the bogie structure where the stress is observed. The reconstructed stresses of reference strain gauges with vertical and lateral identified loads correlate satisfactorily with the measured stresses, which indicates that the identified loads are valid for operational stress recovery.

The measured stress levels during longitudinal calibrations were fairly low, resulting in a worse signal-to-noise ratio. Consequently, the operational longitudinal force estimates included more uncertainties compared with vertical and transversal load estimates. Therefore, longitudinal forces were excluded from the stress recovery process. However, because reconstructed stresses of reference strain gauges without longitudinal forces were relatively close to the measured ones, it can be concluded that the contribution of the longitudinal forces for the bogie stresses were small.

Time Response Assurance Criterion (TRAC) was applied to quantify the degree of correlation between the reconstructed and measured stresses, which is defined by:

$$\boldsymbol{TRAC}_i = \frac{\left(\sum_t \widehat{\boldsymbol{x}}_{m,i}(t)\boldsymbol{x}_{e,i}(t)\right)^2}{\left(\sum_t \widehat{\boldsymbol{x}}_{m,i}(t)\widehat{\boldsymbol{x}}_{m,i}(t)\right)\left(\sum_t \boldsymbol{x}_{e,i}(t)\boldsymbol{x}_{e,i}(t)\right)} \tag{9}$$

where $\widehat{\boldsymbol{x}}_{m,i}(t)$ and $\boldsymbol{x}_{e,i}(t)$ are reconstructed and measured time histories for stress i. TRAC will range from 0 to 1; values closer to 0 indicates poor correlation, and values approaching 1 correspond to perfect correlation. The TRAC values calculated from measurements of about one hour in length during normal driving conditions are presented in Table 1. This period included a wide variety of different types of routes and driving conditions, and it was assumed that it sufficiently covers all relevant driving conditions statistically. These long-term correlation values also confirm the validity of the identified loads.

The most significant sources of stress reconstruction errors are

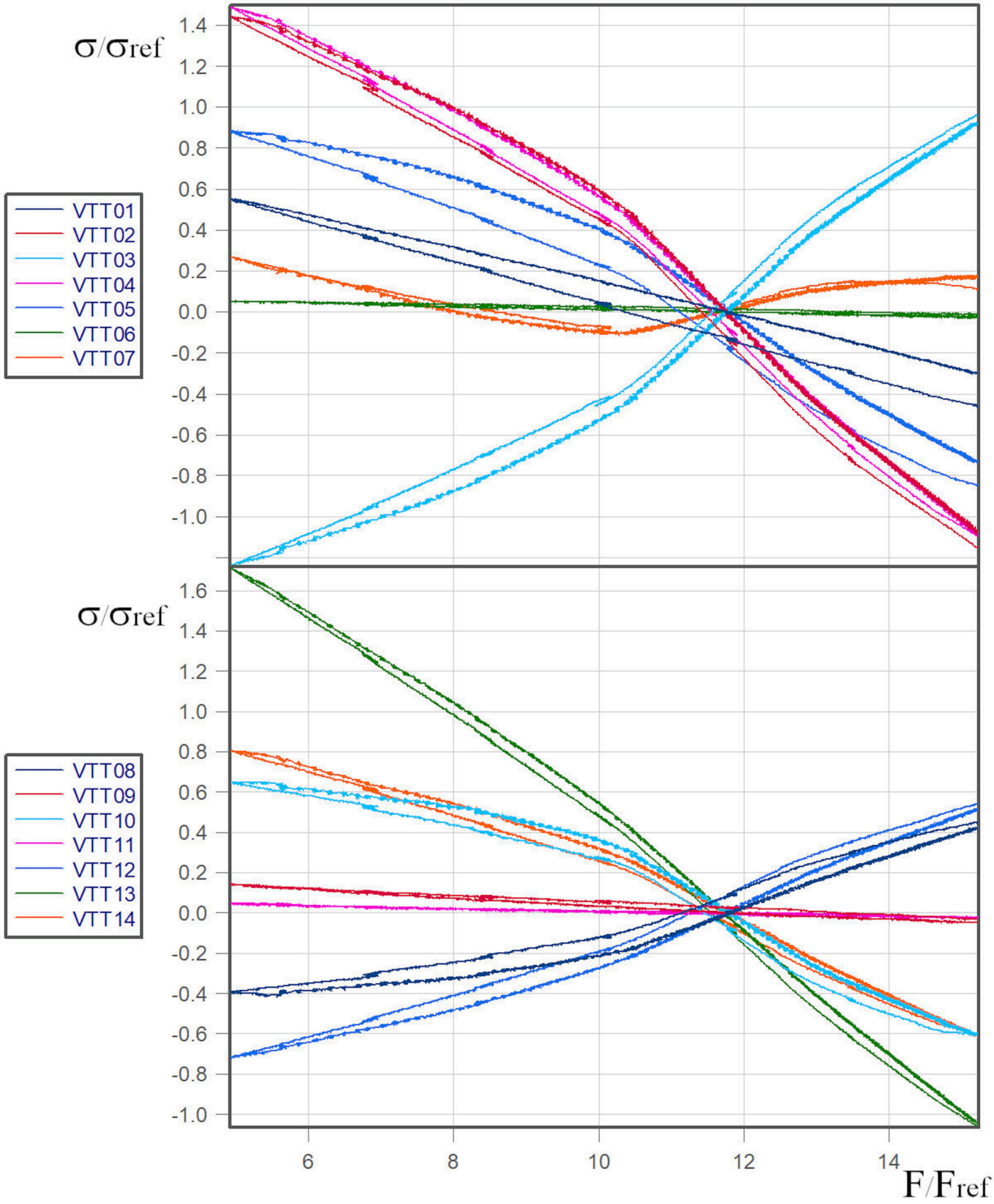

Fig. 6. Linearity check; samples of measured stresses as a function of external calibration force (vertical force for front left wheel). Signals are scaled with reference values measured during normal driving: F_{ref} is the average dynamic amplitude of vertical load of the front left wheel (W1Z) and σ_{ref} is the measured average stress amplitude of strain gauge SGF07. The reference values are calculated from approximately-one-hour long recordings.

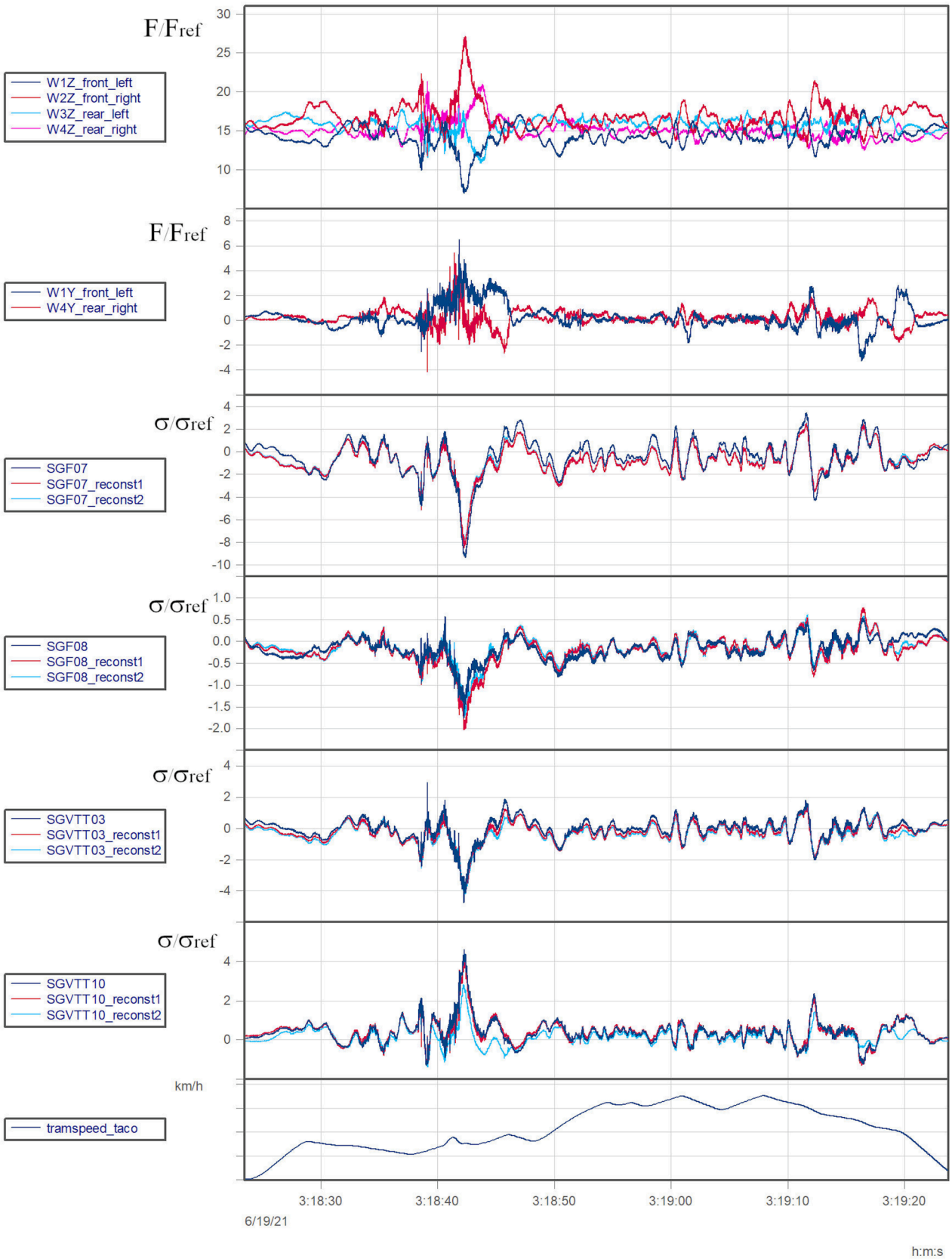

Fig. 7. Identified wheel loads and a comparison of reconstructed stresses with reference strain gauge measurements. Abbreviation "_reconst1" refers to reconstruction with vertical and lateral wheel loads and "_reconst2" refers to reconstruction with vertical loads only. Signals are scaled with reference values: F_{ref} is the average dynamic amplitude of the vertical load of the front left wheel (W1Z), and σ_{ref} is the measured average stress amplitude of strain gauge SGF07. The reference values are calculated from measurements of about one hour in length during normal driving.

Table 1
Degree of correlation between the reconstructed and measured reference stresses (TRAC). The values are determined from measurements of about one hour in length during normal driving.

Reference strain gauge	SGF07	SGF08	SGVTT03	SGVTT10
with vertical and lateral loads (reconst1)	0.940	0.983	0.976	0.993
with vertical loads only (reconst2)	0.939	0.990	0.943	0.895

probably caused by:

i. Non-linearities of the structure of the bogie assembly caused by anti-roll bar, traction bars and primary springs, for example.
ii. In extreme operational loading events during driving, free travel of the secondary springs was exceeded so that the bump stop carried the load. This changed the boundary conditions of the bogie frame and increased uncertainties for the load estimates.
iii. The operational forces caused by dampers were not present during calibrations and, therefore, are not taken into account in the stress reconstruction.
iv. Inertial loads of the traction motor and gearbox were not present during calibrations and are not considered in the stress reconstruction.
v. Longitudinal wheel forces are not included in the stress reconstruction.

However, overall correlation of reconstructed stresses indicated that these phenomena have a limited impact on the stress reconstruction in this type of low-speed railway bogie.

To identify the dynamics of the bogie in a low frequency range, the lowest mode shapes of the bogie were determined experimentally by operational modal analysis (OMA) using acceleration responses recorded during the test trials. The tram modules and bogie under one module were instrumented by capacitive (DC-type) triaxial accelerometers during test trials. A total of nine triaxial accelerometers were installed on the bogie and 18 accelerometers on the tram modules. Natural frequencies, modal damping factors and operational reference factors were identified using the poly-reference least squares complex frequency method (p-LSCF) [17]. The least-squares frequency-domain (LSFD) method was used to identify the mode shapes. It was found that all significant components of the bogie frame stresses appear clearly below the frequency of the lowest elastic mode of the bogie frame (bogie frame twisting). Identified modal damping of this mode was 3 %. Fig. 8 presents the autospectra of measured bogie stresses averaged over measurements of about a minute in length shown in Fig. 7. The abscissa of the graph is relative frequency, which is scaled by the natural frequency of the identified lowest elastic mode of the bogie frame. The frequency of this mode (f_{ref} = 19.4 Hz) is identified by the dashed red line in the graph.

To verify the validity of the reconstructed loads for the fatigue assessment of the bogie frame in the long term, the stress range distribution was calculated using the Rainflow counting method from one-hour long-term measurements. A comparison of Rainflow counts of reconstructed stresses with reference strain gauge measurements indicates relatively good correlation, see Fig. 9. The contribution of the lateral wheel forces for the reconstructed stresses can be seen for the strain gauge location SGVTT10. Generally, the greatest differences for all gauges appear at the lowest bin in the Rainflow spectra. However, the stress range at the lowest bin is so small that when considering appropriate S-N curves, the contribution of these cycles for the cumulative fatigue damage is negligible.

4. Summary and conclusions

In addition to optimal strain gauge placement, the physical calibrations are essential in the strain recovery process to reduce uncertainties of the simulation model, originated from idealisations and uncertainties related to strain gauge placement and orientation accuracy, for example. A novel calibration arrangement was introduced to produce linearly independent load cases for the fully equipped bogie. The boundary conditions of the bogie frame during the calibrations corresponded sufficiently to the normal operational conditions. This is essential for the reliable experimental determination of the influence coefficients between the strain responses and the external loads. The strain reconstruction on the bogie frame was successfully conducted using strain

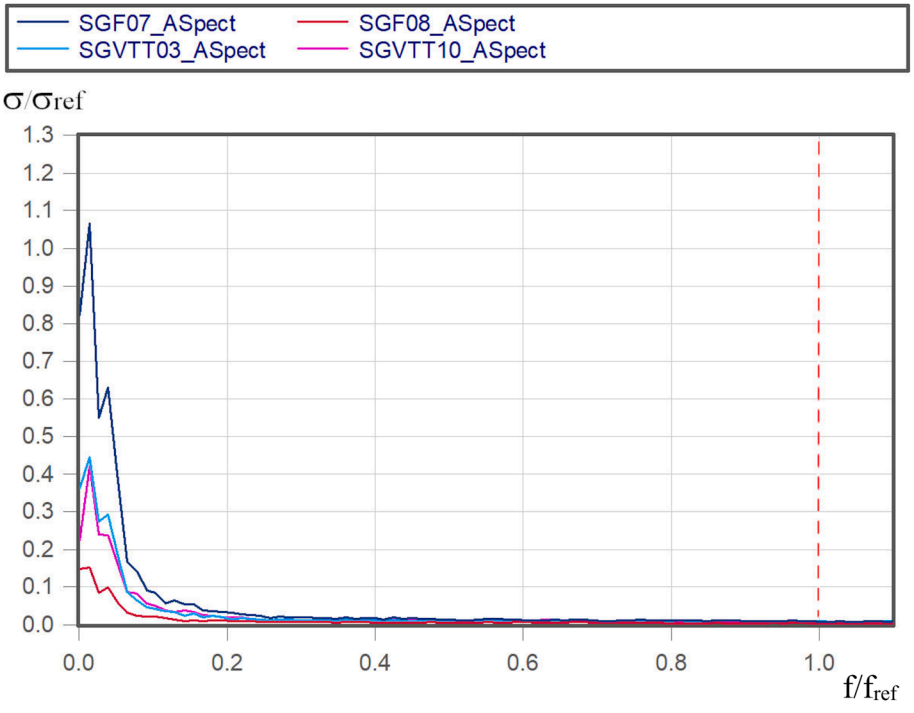

Fig. 8. Autospectra of measured bogie stresses averaged over measurements of about one minute. The frequency of the lowest elastic mode of the bogie frame is shown by the dashed red line. Signals are scaled with reference values: σ_{ref} is the measured average stress amplitude of strain gauge SGF07. The reference values are calculated from measurements of about one minute in length during normal driving. The abscissa of the graph is relative frequency; f_{ref} is the natural frequency of the identified lowest elastic mode of the bogie frame (f_{ref} = 19.4 Hz), shown by the dashed red line in the graph.

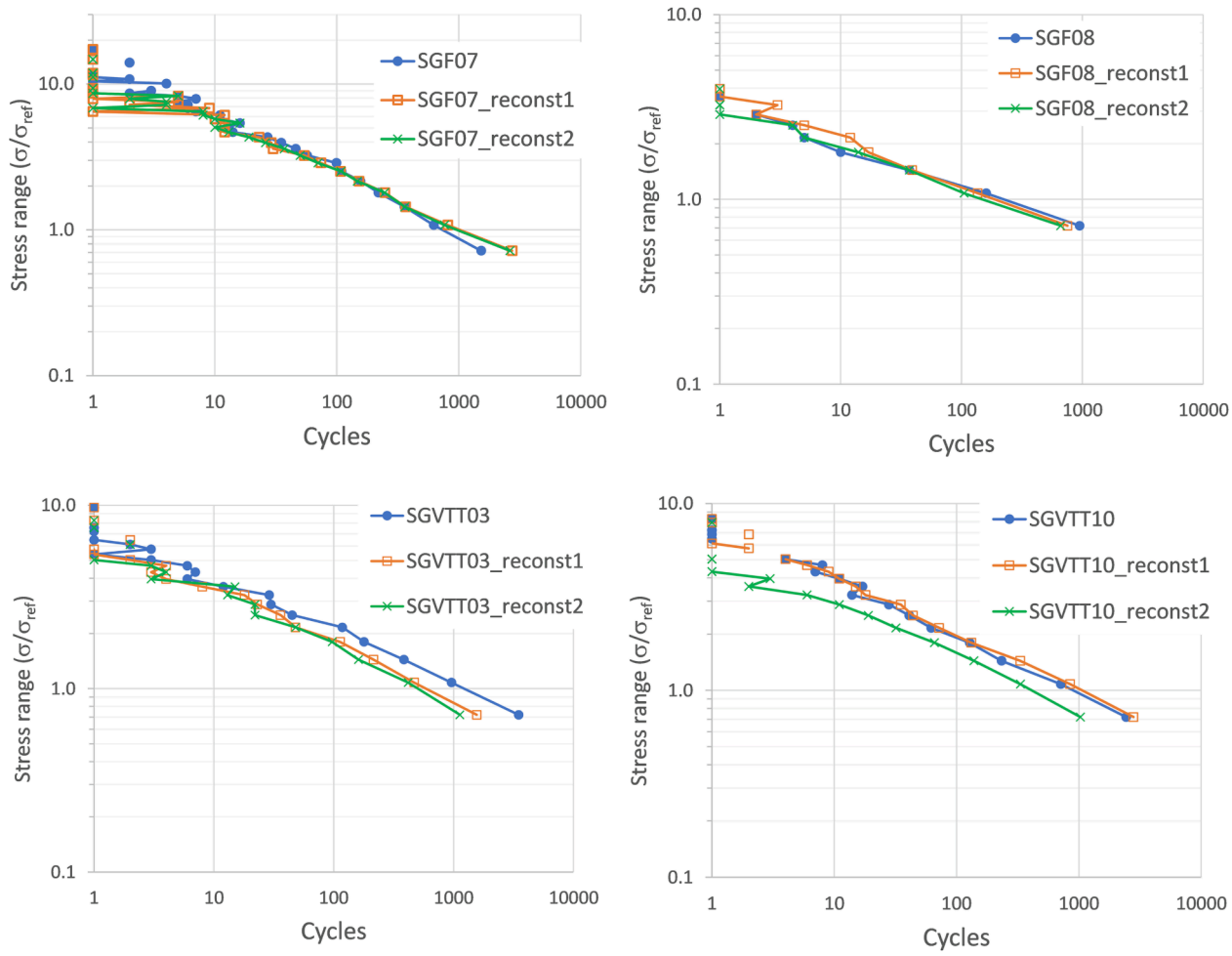

Fig. 9. Comparison of Rainflow counts of reconstructed stresses with reference strain gauge measurements. The abbreviation "_reconst1" refers to reconstruction with vertical and lateral wheel loads and "_reconst2" refers to reconstruction with vertical loads only.

gauges installed only on the bogie frame without a specially instrumented wheelset, for example.

The reconstructed stresses of reference strain gauges correlated satisfactorily with the measured stresses, which indicated that the identified loads are valid for the operational stress recovery and fatigue assessment. This case study indicated that the reconstructed strains on the bogie frame of the tram are valid at low frequency range, where the elastic modes of the bogie frame can be ignored. This method enables the reconstruction of strains of the whole bogie structure from the identified operational loads and provides essential information on the real service load spectrum of the tram, also providing useful data for comparing the different fatigue assessment methods and creating more accurate and realistic stress time histories.

Declaration of Competing Interest

The authors declare that they have no known competing financial interests or personal relationships that could have appeared to influence the work reported in this paper.

Data availability

The data that has been used is confidential.

Acknowledgements

This work was supported by Business Finland under the SmartRail ecosystem projects with Grants 5274/31/2019 and 10966/31/2020.

References

[1] Kassner M. Fatigue strength analysis of a welded railway vehicle structure by different methods. Int J Fatigue 2012;34(1):103–11.
[2] Rennert R. Measured load spectra of rail vehicle car-bodies and their application as design loads. Int J Fatigue 2021;144.
[3] VDV-Schrift 152: Recommendations on the Design for Strength of Urban Rail Rolling Stock according to BOStrab, Verband Deutscher Verkehrsunternehmen, 2016.
[4] Wu X, Gao A, Wen Z, Wu S, He S, Chi M, et al. Online estimation of fatigue damage of railway bogie frame based on axle box accelerations. Veh Syst Dyn 2022.
[5] Wang BJ, Xie SQ, Li Q, Ren ZS. Fatigue damage prediction of metro bogie frame based on measured loads. Int J Fatigue 2022;154.
[6] Ji C, Sun S, Li Q, Ren Z, Yang G. Realistic fatigue damage assessment of a high-speed train bogie frame by damage consistency load spectra based on measured field load. Measurement 2020;166.
[7] Matsumoto A, Sato Y, Ohno H, Shimizu M, Kurihara J, Tomeoka M, et al. Continuous observation of wheel/rail contact forces in curved track and theoretical considerations. Veh Syst Dyn 2012;50:349–64.
[8] Urda P, Muñoz S, Aceituno JF, Escalona JL. Wheel-rail contact force measurement using strain gauges and distance lasers on a scaled railway vehicle. Mech Syst Sig Process 2020;138.
[9] Xia F, Cole C, Wolfs P. Grey box-based inverse wagon model to predict wheel–rail contact forces from measured wagon body responses. Veh Syst Dyn 2008;46:469–79.
[10] Sun YQ, Cole C, Spiryagin M. Monitoring vertical wheel–rail contact forces based on freight wagon inverse modelling. Adv Mech Eng 2015;7(5):1–11.
[11] Weia L, Zenga J, Wua P, Gaoa H. Indirect method for wheel–rail force measurement and derailment evaluation. Veh Syst Dyn 2014;52(12):1622–41.
[12] Dhingra AK, Hunter TG, Gupta DK. Load Recovery in Components Based on Dynamic Strain Measurements. J Vib Acoust 2013;135(5):pp.

[13] Mitchell TJ. An Algorithm for the Construction of "D-Optimal" Experimental Designs. Technometrics 1974;16(2):203–10.
[14] Nieminen V, Sopanen J. Optimal sensor placement of triaxial accelerometers for modal expansion. Mech Syst Sig Process 2023;184.
[15] Tarpø M, Nabuco B, Georgakis C, Brincker R. Expansion of experimental mode shape from operational modal analysis and virtual sensing for fatigue analysis using the modal expansion method. Int J Fatigue 2020;130.
[16] Augustine P, Hunter T, Sievers N, Guo X. Load Identification of a Suspension Assembly Using True-Load Self Transducer Generation, SAE Technical Paper 2016-01-0429, doi:10.4271/2016-01-0429, 2016.
[17] Peeters B, Van der Auweraer H. Polymax: A revolution in operational modal analysis. 1st International Operational Modal Analysis Conference, Denmark, Copenhagen. 2005.